Article

Synthesis of Asymmetrical $CsPbBr_3/TiO_2$ Nanocrystals with Enhanced Stability and Photocatalytic Properties

Wanli Liu [1], Jinfeng Liu [1], Xiaoqian Wang [1], Jiazhen He[1], Yuqing Li [1], and Yong Liu [1]*

[1]International School of Materials Science and Engineering (ISMSE), State Key Laboratory of Advanced Technology for Material Synthesis and Processing, Wuhan University of Technology, Wuhan 430070, China; liuwani97@163.com.

* Correspondence: liuyong3873@whut.edu.cn

Abstract: Practical applications of $CsPbX_3$ nanocrystals (NCs) are limited by their poor stability. The formation of heterojunction between $CsPbX_3$ NCs and oxides is an effective means to protect perovskite from polar solvents and other external factors. Significantly improving the stability and photocatalytic properties of the core/shell perovskite is very important for its application in photoelectric and photocatalytic technology. Here, we report the synthesis of asymmetrical $CsPbBr_3/TiO_2$ core-shell heterostructure NCs at single particle level by hot injection liquid phase synthesis and sol-gel method, where each $CsPbBr_3$ NCs is partially covered by titanium dioxide. It is shown that the type II arrangement is generated at the heterogeneous interface, which greatly facilitates the separation of electron-hole pairs and increases the carrier transport efficiency. More crucial, due to the protection of titanium dioxide shell, the product has higher long-term stability in humid air compared with bare $CsPbBr_3$ NCs. The asymmetrical core-shell heterostructure prepared in this study not only improves the stability of $CsPbX_3$ NCs, but also provides some ideas for optoelectronic device applications and TiO_2-based photocatalysts.

Keywords: perovskite; core-shell; heterostructure; stability; photocatalyst

1. Introduction

$CsPbBr_3$ is a typical metal halide perovskite material that has become one of the most promising materials for optoelectronic applications, including solar cells[1-4], light emitting diodes (LED)[5-10], photodetectors[11], and lasers[12-16]due to its excellent photoelectric and catalytic properties such as narrow optical emission range, high photoluminescent quantum yield(PLQY), high photogenerated charge mobility and tunable band gap. In recent years, the rapid development of research in this field has led to significant advances in the study of optoelectronic properties and materials. Inspired by the results of photovoltaic applications, $CsPbBr_3$ NCs is a potential candidate for conducting efficient photocatalysis[17, 18]. Since the pioneering work reported by Kovalenko et al [19] in 2015, significant progress has been made in the preparation methods and photocatalytic applications of $CsPbX_3$ NCs.

However, perovskite is often described as a crystalline liquid due to the soft and dynamic properties of the crystal lattice, so light-induced carriers are less likely to be trapped and scattered. At room temperature, polarons are formed by the coupling of electrons and holes, caused by the ionic properties and strong structural dynamics of the PbX lattice, thus shielding the Coulomb potential and reducing the charge capture and scattering between polarons and between polarons and charged defects or optical phonons. Although there is a high defect tolerance in the lead halide perovskite NCs materials, its defects will still reduce its luminous performance. The high photoluminescence quantum yield of perovskite can only achieve 80-90% in the green-red fluorescence range of the spectrum. In addition, as an ionic crystal, perovskite NCs is not very stable in the process of purification

 doi:10.20944/preprints202306.0442.v1

and storage under harsh environmental conditions (such as air, polar solvents, heat and light). They usually decompose or dissolve quickly, which greatly limits its practical application in photoelectric devices, catalysis and other fields. The interaction between ligands and atoms on the perovskite NCs surface is highly dynamic. During purification, surface ligand shedding caused by polar solvents leads to an increase in nanocrystal defects, resulting in decomposition and loss of fluorescence properties. In recent years, researchers have proposed many methods to solve the worldwide problem of poor stability of metal halide perovskite, such as surface modification, polymer encapsulation, silicon coating, atomic layer deposition passivation, etc. Although surface passivation by organic ligands or polymers can significantly improve the stability of perovskites, these insulating shells severely limit the charge transport of metal halide perovskite themselves for optoelectronic, catalytic and other applications.

In addition to polymers [20-27]and inert shell layers[16, 28-32], semiconductors were also introduced to improve the stability and photophysical properties of perovskite. More importantly, by using another semiconductor with different conduction and valence bands, one can easily tune the bandgap or charge transfer processes and thus improve the photophysical properties. Prior to shell growth of perovskite NCs, shell materials were carefully selected to design the core-shell structure to allow for favorable band arrangement. In type I core-shell structures, the shell material has a wider energy band gap than the core, so the edges of the core material of the conduction and valence bands are located in the energy gap of the shell, resulting in electrons and holes locally in the core. The band gap of the core material determines the band gap energy of this heterogeneous structure, while the shell provides passivation of surface defects and limits electrons and holes within the core. This can improve the overall optical properties and stability of NCs. Type II structures have a staggered arrangement in which the edges of the valence and conduction bands of the core material have lower or higher energies than the edges of the shell material. The band gap of type II structures is determined by the energy separation between the conduction band edge of one semiconductor and the valence band edge of another semiconductor. Carriers are spatially separated in these structures, thus offering potential benefits for applications such as optoelectronics and photocatalysis. TiO_2, as a chemically inert and nontoxic photocatalyst, forms a type II heterojunction between $CsPbX_3$, which can not only solve the problem of stability, but also improve the charge transfer efficiency of perovskite, laying a foundation for its photoelectric and photocatalytic applications.

The sol-gel method has been widely used for the modification of perovskite nanoparticles with various oxide materials such as silica and titanium dioxide. However, since $CsPbBr_3$ NCs are very sensitive to water and temperature and fluorescence of perovskites quenching occurs before the formation of silica or titanium oxide shell layers, it is challenging to modify their surfaces using conventional sol-gel methods. In the available reports, Li et al.[33] demonstrated that TiO_2 shell coating, which improved the stability of perovskite, but resulted in partial decomposition of $CsPbBr_3$ NCs or dissolution of corners and edges during hydrolysis and calcination. Ji et al. [34] studied the synthesis of highly stable $CsPbBr_3/TiO_2$ nanocomposites by a top-assisted low temperature solvothermal method. Although the material improves the stability of the perovskite NCs and preserves the edge of the perovskite core from being destroyed, the agglomeration is severe and the size is large, which poses obstacles for the photoelectric and photocatalytic applications. For example, in perovskite light emitting diodes (PeLED) applications, small size particles facilitate the formation of thin films with high uniformity. Therefore, we are eager to develop a method that can achieve heterogeneous coating of $CsPbBr_3$ with TiO_2 at the single-particle level to improve stability.

Herein, we certify the synthesis of an asymmetric $CsPbBr_3/TiO_2$ core-shell nanocrystals heterojunction at the single-particle level in anhydrous solvent and at low temperature, aiming to improve the stability of perovskite, thereby improving its photoelectric and photocatalytic performance. Based on the band alignment, it is confirmed that the

 doi:10.20944/preprints202306.0442.v1

obtained $CsPbBr_3/TiO_2$ heterojunction NCs has a type-II heterostructure with enhanced carrier transport efficiency. It is demonstrated that the $CsPbBr_3/TiO_2$ NCs show good optoelectronic properties and enhanced water stability under water test conditions, which provide a reference value for the preparation of high-efficiency, long-life photovoltaic and luminescent devices.

2. Results and Discussion

Firstly, cesium precursor (cesium oleate) was prepared by using cesium carbonate as cesium source, adding oleic acid and trin-octylphosphine ligand as raw materials. Then lead bromide precursor was prepared by adding octadecene, oleic acid and oleamine to dissolve lead bromide powder. Cesium oleate was injected into the lead bromide precursor by hot injection method. After a few seconds of reaction, the reaction solution was cooled to room temperature in an ice bath and centrifugally washed to obtain $CsPbBr_3$ NCs. Next, we chose titanium butoxide as the titanium precursor, slowly dropped the diluted titanium precursor into the toluene solution of $CsPbBr_3$ NCs at a certain speed, and stirred the solution at room temperature for 3 h. The hydrolysis reaction occurred, so that TiO_2 was deposited on the surface of $CsPbBr_3$ NCs, and then the reaction solution was placed in a Teflon-lined stainless steel autoclave for 10 h, and the $CsPbBr_3/TiO_2$ light yellow powder was obtained by centrifugation and drying (see Methods section for details).

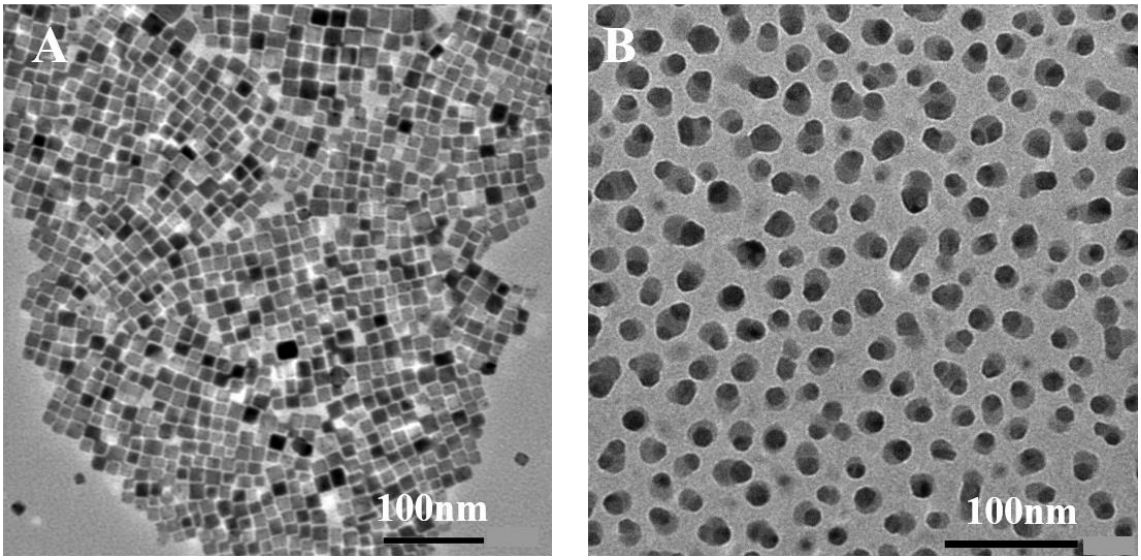

Figure1. (A-B) Transmission electron microscopy (TEM) images of $CsPbBr_3$ NCs and asymmetrical $CsPbBr_3/TiO_2$ NCs, respectively.

The morphologies of $CsPbBr_3$ NCs and asymmetrical $CsPbBr_3/TiO_2$ NCs were analyzed by transmission electron microscopy (TEM). As shown in Figure 2A, the $CsPbBr_3$ NCs materials exhibit highly uniform monodispersion with clear edges and uniform size with an edge length of about 17 nm, indicating the preparation of high-quality perovskite nanocrystals. Figure 2B is the TEM image of asymmetrical $CsPbBr_3/TiO_2$ core-shell NCs. It can be obviously observed that each nanocrystalline particle has two regions with different image contrast, indicating that the material is composite structure. $CsPbBr_3/TiO_2$ NCs are composed of two different structural components, $CsPbBr_3$ and TiO_2, with an obvious heterogeneous interface, in which the dark part is $CsPbBr_3$ NCs, and the light part is TiO_2, which further indicates the formation of core-shell heterojunction. Importantly,

Preprints (www.preprints.org) | NOT PEER-REVIEWED | Posted: 6 June 2023 doi:10.20944/preprints202306.0442.v1

after the titanium oxide coating, the edges of the perovskite are not dissolved, achieving precise coating at the single-particle level. and the distribution of these elements

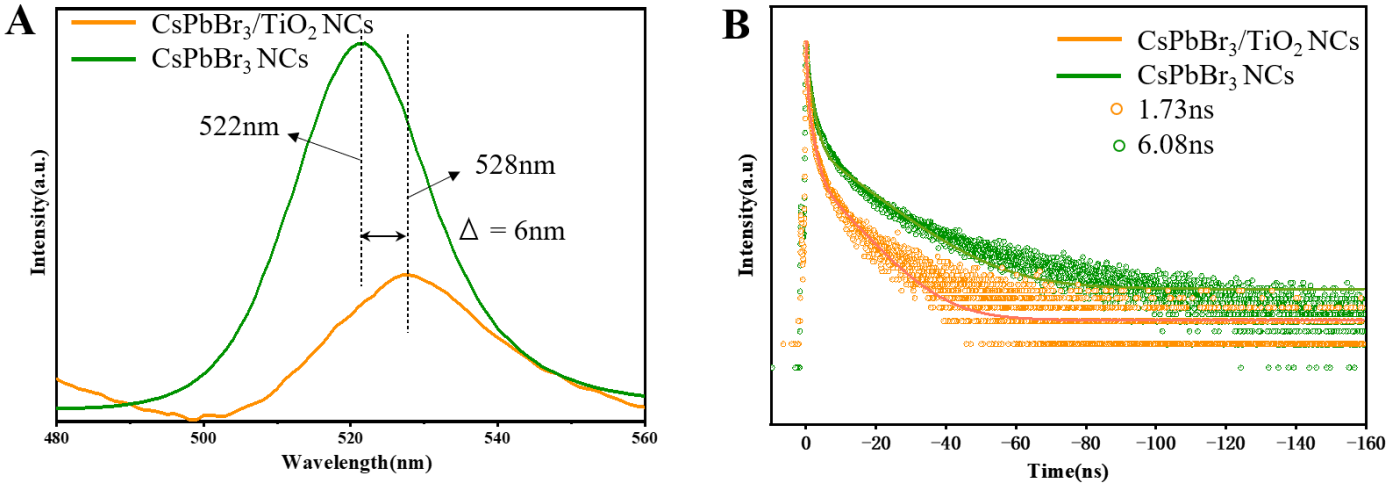

Figure2. (A) Photoluminescence (PL) spectra and (B) PL time-resolved photoluminescence (TRPL) spectra of $CsPbBr_3$ NCs and asymmetrical $CsPbBr_3/TiO_2$ NCs.

Since most applications of perovskite are related to its photoelectric and catalytic properties, it is desirable that materials have both environmental stability and efficient charge transport. To gain more insight into the material charge transfer kinetics, we recorded the photoluminescence (PL) emission spectra and time-resolved photoluminescence spectra (TRPL) of $CsPbBr_3$ NCs and asymmetrical $CsPbBr_3/TiO_2$ NCs (Figure 2). As shown in the figure 2A, it can be observed that the photoluminescence emission peaks of $CsPbBr_3$ NCs and $CsPbBr_3/TiO_2$ NCs at about 522 nm and 528nm, respectively. Compared to $CsPbBr_3$ NCs, the PL peak of $CsPbBr_3/TiO_2$ NCs is slightly red shifted by 6 nm. After TiO_2 shell coating, the PL intensity decreases. Figure 2B shows the TRPL of $CsPbBr_3$ NCs and asymmetrical $CsPbBr_3/TiO_2$ NCs. The fitted decay curves reveal that the $CsPbBr_3/TiO_2$ NCs (τ=1.73 ns) have shorter carrier lifetime compared to $CsPbBr_3$ (τ=6.08 ns), and the decreased PL lifetime indicates improved charge diffusion and separation, the rapid charge transfer from $CsPbBr_3$ NCs to the TiO_2 shell, thus leading to enhanced photovoltaic performance. The reduced fluorescence lifetime further manifests that after TiO_2 shell coating, the $CsPbBr_3/TiO_2$ core/shell NCs generate a new nonradiative path, probably electron transfer from the conduction band of $CsPbBr_3$ NCs to the conduction band of titanium dioxide [35], indicating the formation of type II heterojunctions, which greatly facilitate the separation of electron-hole pairs, and $CsPbBr_3/TiO_2$ NCs with higher carrier mobility.

To confirm our hypothesis, we investigated the electronic energy band structures of $CsPbBr_3$ NCs and asymmetrical $CsPbBr_3/TiO_2$ NCs using Ultraviolet-visible absorption spectroscopy (UV-Vis). Compared with the normal hydrogen electrode (NHE), the conduction band and valence band edge of $CsPbBr_3$ NCs are ≈-3.37eV and ≈−5.79 eV, respectively. The conduction and valence bands of $CsPbBr_3$ are higher than those of titanium dioxide. Therefore, a type II band arrangement can be formed in the $CsPbBr_3/TiO_2$ heterostructure NCs. In this case, the lowest energy hole should be confined to the $CsPbBr_3$ nucleus, and electrons can delocalize on the $CsPbBr_3$ nucleus and the titanium dioxide shell, thus promoting charge transfer and reducing PLQY. From the UV-Vis absorption spectra (Figure 3A), it is clear that $CsPbBr_3$ NCs and $CsPbBr_3/TiO_2$ NCs showed significant absorption peaks in ultraviolet range. Based on Einstein's photoelectric effect and the Kubelka-Munk equation [36], the surface optical band gaps of $CsPbBr_3$ NCs and $CsPbBr_3/TiO_2$ NCs were estimated to be 2.42 eV and 2.40 eV(Figure 3B), respectively, by extrapolating the linear region of the absorption edge in the UV-Vis spectrum to the energy

Preprints (www.preprints.org) | NOT PEER-REVIEWED | Posted: 6 June 2023 doi:10.20944/preprints202306.0442.v1

axis intercept. The reduction of the electron transition band gap is consistent with the fluorescence lifetime results, which further proves that the charge transport characteristics of perovskite nanocrystals are optimized after titanium oxide coating. The work function (Φ) is another important parameter in the study of electron transfer in duplicate semiconductor heterojunctions. It can be calculated from the energy difference of surface valence band maximum and the Fermi level of the material. Based on UPS and UV-Vis data, the work functions of anatase TiO_2 and $CsPbBr_3$ NCs are calculated to be 6.0 eV and 4.58 eV, respectively, indicating that the Fermi level of anatase TiO_2 is lower than that of $CsPbBr_3$ NCs. When they come into contact, electrons flow from $CsPbBr_3$ to anatase titanium dioxide, making the same Fermi level consistent and producing internal electric field at the $CsPbBr_3/TiO_2$ NCs interface. These results are consistent with the results of the fluorescence lifetime test. The coating of titanium oxide is beneficial to charge separation in perovskite and improves the catalytic activity.

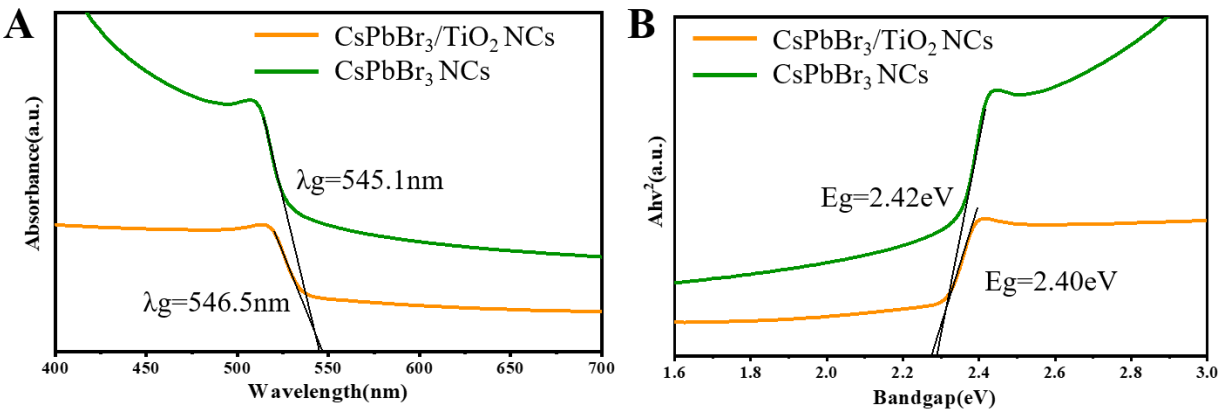

Figure3. (A) Ultraviolet-visible spectroscopy (UV-Vis) of $CsPbBr_3$ NCs and asymmetrical $CsPbBr_3/TiO_2$ NCs. (B)Absorbance versus photon energy and the determined bandgap Eg of $CsPbBr_3$ NCs and asymmetrical $CsPbBr_3/TiO_2$ NCs.

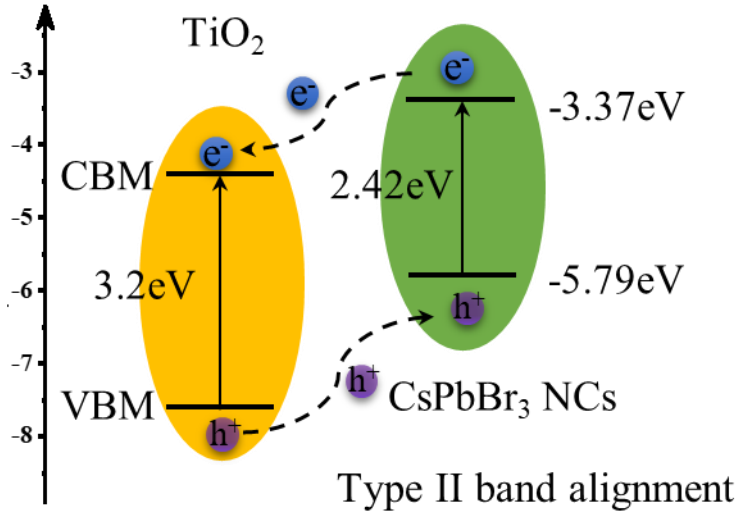

Figure4. Bandgap distribution of $CsPbBr_3$ as well as TiO_2 in this system.

Based on the energy levels of $CsPbBr_3$ NCs and TiO_2 NCs, an energy band structure diagram is proposed as shown in Figure 6. From the band alignment, it was found that a type II nanocomposite was formed, in which both the conduction band and valence band levels of the semiconductor $CsPbBr_3$ were higher than those of the semiconductor titanium dioxide. Once irradiated by light (λ = 546.5 nm), electrons in the valence band of $CsPbBr_3$

 doi:10.20944/preprints202306.0442.v1

leap to the conduction band and form holes in their original positions. Under the action of the internal electric field, the carriers generated and leapt to the depletion region will be separated rapidly in the heterojunction, where the electrons will move toward the TiO_2 conduction band and the holes will transport to $CsPbBr_3$, and the photocurrent output due to the photoresponse can be obtained through the electrochemical workstation. The holes from the TiO_2 valence band will be transferred to the $CsPbBr_3$ valence band under the action of external electric field, and the electrons will migrate in the opposite direction, thus producing a stable photoresponse, and the optical signal will be converted into an electrical signal.

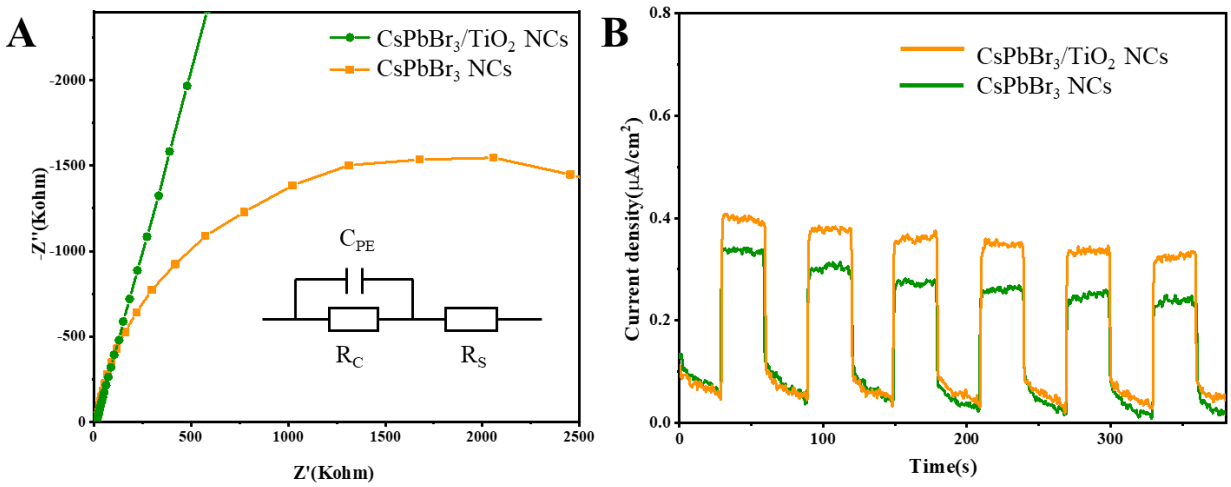

Figure5. (A) Electrochemical impedance spectra (Nyquist plot) of $CsPbBr_3$ NCs and $CsPbBr_3/TiO_2$ NCs, inset is the equivalent circuit model and *Z'* and *-Z* 'are the virtual and real impedances, respectively. (B) Transient photocurrent responses to on-off illumination of $CsPbBr_3$ NCs and $CsPbBr_3/TiO_2$ NCs electrodes at -0.1 V versus NHE in neutral water (0.5M Na_2SO_4).

The electrochemical impedance spectra (ESI) and the photoresponsive current densities of $CsPbBr_3$ NCs and $CsPbBr_3/TiO_2$ NCs materials were tested as shown Figure 5. The charge transport properties of $CsPbBr_3$ NCs and $CsPbBr_3/TiO_2$ NCs were further investigated by photoelectrochemical studies. The Nyquist plot is generally used in EIS and the Nyquist plot of the most common equivalent circuit model is semicircular in shape. The diameter of the semicircle is equal to the carrier migration resistance, and the smaller the diameter of the semicircle, the larger the carrier migration rate. As shown in the Figure 5A, compared with $CsPbBr_3$ NCs, $CsPbBr_3/TiO_2$ NCs possess a smaller semicircle arc. The results show that with the formation of TiO_2 shells, the charge transfer resistance of the $CsPbBr_3/TiO_2$ NCs is significantly reduced. In order to record the photocurrent generated by the photoresponse and exclude the effect of other factors, the light source is usually switched on at certain intervals to record the photocurrent profile. As shown in the Figure 8B, when the light source was turned off, the recorded photocurrent density was almost zero; when the light source was turned on after 30 s, the current instantaneously increased; and when the light source was turned off at an interval of 30 s, the current instantaneously decreased. Compared with $CsPbBr_3$ NCs, $CsPbBr_3/TiO_2$ NCs have higher current density. This result further confirms that the formation of heterostructure between $CsPbBr_3$ and TiO_2 improves the carrier migration efficiency of the perovskite material and has better charge transport properties.

3. Materials and Methods

3.1 Materials

The cesium carbonate (Cs_2CO_3, 99.9% metals basis, Aladdin), oleic acid (OA, 80-90%, Aladdin), oleylamine (OAm, 80-90%, Aladdin), titanium butoxide ($C_{16}H_{36}O_4Ti$, TBOT,

 doi:10.20944/preprints202306.0442.v1

>99.0%, Aladdin), trinoctylphosphine (TOP, 90%, Aladdin), 1-octadecene (ODE, >90% (GC), Aladdin), lead (II) bromide ($PbBr_2$, 99.0%, Aladdin). The toluene was purchased from Sinopharm Chemical ReagentCo.

3.2 Methods

Preparation of Cesium Oleate: In a typical synthesis, 400 mg of Cs_2CO_3 (1.23 mmol), 15 mL ODE, 2 mL TOP and 1.25 mL oleic acid were added into a 25 mL three-neck round bottom flask connected with a double row of tubes and dried under N_2 at 120 °C for 1 h In the oil bath until Cs_2CO_3 reacts with OA to form cesium oleate (Cs-OA). The Cs-OA solution was stored at room temperature and preheated to 140℃ before synthesis of $CsPbBr_3$ nanocrystals.

Synthesis and Purification of $CsPbBr_3$ NCs: Briefly, 138 mg of $PbBr_2$ (0.374 mmol) was mixed with 10.0 mL ODE in another 25 mL three-neck round bottom flask connected with a double row of tubes, and was dried under vacuum at 120 °C for 1 h.Then, 1.0 mL OAm and 1.0 mL OA were slowly added into the flask under the N_2 atmosphere. After the solution became clear, the temperature was raised to 170 °C, followed rapidly injection of 0.8 mL of Cs-OA. After 5 s solution turns yellow, the reaction was quenched by immersing the flask into an ice-water bath. The quenched solution was centrifuged at 10000 rpm for 5 min. To remove supernatant, the centrifuged $CsPbBr_3$ NCs were dispersed in 5 mL dry toluene, were washed twice with dry toluene and dispersed into 25 mL of dry toluene for further use.

Preparation of asymmetrical $CsPbBr_3$ /TiO_2 heterojunction: Typically, when the stirring rate of the reaction system is 1500 rpm, titanium butoxide solution (80 μL titanium butoxide /2 mL dry toluene) was added to 10 mL $CsPbBr_3$ NCs toluene solution. After stirring for 3 h, the reaction solution was transferred into a Teflon-lined stainless steel autoclave, and then the solvothermal reaction process was carried out at 160 °C for 10 h. After cooling down to room temperature, the obtained product was centrifuged at 10000 rpm for 5 min to collect precipitates, washed twice with dry toluene and dried at 40 °C for 6 h, then ground to obtain asymmetrical $CsPbBr_3$ /TiO_2 powder sample.

3.2 Characterization

3.2.1. Materials Characterization

Transmission Electron Microscopy (TEM) Characterization. TEM images were acquired on a JEOL JEM-1400 Plus electron microscope equipped with a thermionic gun at an accelerating voltage of 120 kV. The samples of $CsPbBr_3$ NCs and $CsPbBr_3$/TiO_2 NCs were prepared by depositing a diluted nanocrystal suspension in toluene onto carbon-coated copper grids.

3.2.2. Optical Characterization

UV–Vis absorption spectra of $CsPbBr_3$ NCs and $CsPbBr_3$/TiO_2 NCs samples was collected by Shimadzu UV-3600. The steady-state photoluminescence (PL) spectra and steady-state and time-resolved photoluminescence (TRPL) spectra were measured on a Shimadzu RF-6000 spectrophotometer with LabSolutions RF software using an excitation wavelength (λex) of 420 nm for $CsPbBr_3$ NCs and the asymmetrical $CsPbBr_3$/TiO_2 NCs. Nanocrystals samples were prepared by diluting NCs solutions in toluene in quartz cuvettes with a path length of 10 mm.

3.2.3. (Photo)electrochemistry Characterization

For (photo)electrochemistry measurement, a Zennium electrochemical workstation (Germany, Zahner Company) was used, and the measurement was performed in a three-electrode setup with the working electrode of the sample electrode, counter electrode of platinum disk, and reference electrode of Ag/AgCl (saturated KCl). (EAg/AgCl=+0.1989V vs. NHE) in the (photo)electrochemical electrolyte (0.5 M Na_2SO_4). For photocurrent measurement, the light source was a 405 LED, the light intensity was tested with a Newport photometer. Electrochemical impedance spectra were measured in 0.5 M Na_2SO_4 at -0.1 V vs. NHE with an amplitude of 10 mV (Frequency: 100 mHz–20 kHz).

 doi:10.20944/preprints202306.0442.v1

5. Conclusions

In summary, $CsPbBr_3$ NCs were firstly prepared by thermal injection liquid-phase synthesis, and then asymmetrical $CsPbBr_3$ /TiO_2 core-shell NCs were synthesized by sol-gel method. The prepared $CsPbBr_3$ NCs were uniformly distributed, homogeneous in size and highly monodisperse with size around 17 nm. TEM images of asymmetrical $CsPbBr_3$ /TiO_2 core-shell NCs materials clearly show that the $CsPbBr_3$ and TiO_2 materials are distributed in different regions with different image contrast, indicating the formation of heterogeneous structures. The red shift of 6nm of photoluminescence emission peak, the decrease of photoluminescence emission peak and fluorescence lifetime are due to the difference of grain size and charge migration between $CsPbBr_3$ and TiO_2. The work function calculation shows that the Fermi level of anatase TiO_2 is lower than that of $CsPbBr_3$ NCs. When they touch each other, electrons flow from $CsPbBr_3$ to anatase titanium dioxide, making the same Fermi level consistent. The energy band structures of the materials were obtained by UV-Vis analysis, demonstrating that asymmetrical $CsPbBr_3$ /TiO_2 NCs form a type II heterostructure with narrower forbidden band widths and the shorter carrier migration paths, as well as higher carrier mobilities. By measuring the electrochemical impedance and photocurrent density of $CsPbBr_3$ NCs and asymmetrical $CsPbBr_3$/TiO_2 NCs, it is further verified that asymmetrical $CsPbBr_3$/TiO_2 NCs have better carrier transport properties compared to $CsPbBr_3$ NCs. This work provides a low-cost and easy-to-handle method to achieve good water stability and excellent optoelectronic properties of perovskite, which shows promising applications in photocatalysts and high-performance optoelectronic devices.

Supplementary Materials: No supporting information in this article.

Author Contributions: Y.L. conceived project ideas and material synthetic designs. W.L.L., J.F.L., X.Q.W., Y.Q. L. and J.Z.H performed material characterization and data analysis. Y. L., and W.L.L. discussed the results and contents for this work. W.L.L. and Y.L. wrote the original drafts, reviews, and edits. All authors have read and agreed to the published version of the manuscript.

Funding: This research was funded by National Natural Science Foundation of China (52072281, Y.L.); The Major Program of the National Natural Science Foundation of China (22293021, Y.L.); the National innovation and entrepreneurship training program for college students (No. S202210497011 Y.L.). Y.L. gratefully acknowledges Youth Innovation Research Fund project of State Key Laboratory of Advanced Technology for Materials Synthesis and Processing, Wuhan University of Technology.

Data Availability Statement: Data available in a publicly accessible repository that does not issue DOIs or on request from the corresponding author.

Acknowledgments: The authors thank to the Analytical and Testing Centre of Wu-han University of Technology is acknowledged for the UV-Vis characterizations.

Conflicts of Interest: The authors declare no conflict of interest.

References

1. Kojima, A.;Teshima, K.;Shirai, Y.;Miyasaka, T. Organometal halide perovskites as visible-light sensitizers for photovoltaic cells. *J. Am. Chem. Soc.* **2009,** *131*, 6050-1.
2. Jeon, N. J.;Noh, J. H.;Yang, W. S.;Kim, Y. C.;Ryu, S.;Seo, J.;Seok, S. Compositional engineering of perovskite materials for high-performance solar cells. *Nature.* **2015**, 476-480.
3. Swarnkar, A.;Marshall, A. R.;Sanehira, E. M.;Chernomordik, B. D.;Moore, D. T.;Christians, J. A.;Chakrabarti, T.;Luther, J. Quantum dot-induced phase stabilization of α-$CsPbI_3$ perovskite for high-efficiency photovoltaics. *Science* **2016,** *354*, 92-95.
4. Yang, W. S.;Park, B. W.;Jung, E. H.;Jeon, N. J.;Kim, Y. C.;Lee, D. U.;Shin, S. S.;Seo, J.;Kim, E. K.;Noh, J. H. J. S., Iodide management in formamidinium-lead-halide–based perovskite layers for efficient solar cells. *Science.* **2017,** *356*, 1376-1379.
5. Song, J.;Li, J.;Li, X.;Xu, L.;Dong, Y.;Zeng, H. Quantum dot light-emitting diodes based on inorganic perovskite cesium lead halides ($CsPbX_3$). *Adv. Mater.* **2016,** *27*, 7162-7167.
6. Li, J.; Wang, S.; Chen, J.; Dong, J.; Shan, Y.V50-fold EQE improvement up to 6.27% of solution-processed all-inorganic perovskite $CsPbBr_3$ QLEDs via surface ligand density control. *Adv. Mater.* **2017,** *29*.1603885.

7. Zhi-Kuang, T.;Reza Saberi, M.;May Ling, L.;Pablo, D.;Ruben, H.;Felix, D.; Michael, P.;Aditya, S.;Pazos, L. M.;Dan, C. Bright light-emitting diodes based on organometal halide perovskite. *Nat. Nanotechnol.* **2018,** *9*, 687-692.
8. Zhang, X.;Xu, B.;Zhang, J.;Gao, Y.;Zheng, Y.;Wang, K.;Sun, X. All-inorganic perovskite nanocrystals for high-efficiency light emitting diodes: dual-phase $CsPbBr_3$-$CsPb_2Br_5$ Composites. *Adv. Funct. Mater.* **2016,** *26*, 4595-4600.
9. Song, T.;Cheng, H.;Fu, C.;He, B.;Zou, B. Influence of the active layer nanomorphology on device performance for ternary PbS_xSe_{1-x} quantum dots based solution-processed infrared photodetector. *Nanotechnology* **2016,** *27*, 165202.
10. Chiba, T.;Hoshi, K.;Pu, Y. J.;Takeda, Y.;Kido, J. High efficiency perovskite quantum-dot light-emitting devices by effective washing process and interfacial energy level alignment. *ACS Appl. Mater. Inter.* **2017,** *9*, 18054.
11. Dong, Y.; Gu, Y.;Zou, Y.;Song, J; Xu, L;Li, H. Improving all-inorganic perovskite photodetectors by preferred orientation and plasmonic effect. *Small* **2016,** *12*, 5622-5632.
12. Chien, T.;Mathews;Nripan;Yantara;Natalia;Mingjie;Mhaisalkar;Subodh, G.;Boix;Pablo, P., Perovskite materials for light-emitting diodes and lasers. *Adv.Mater.* **2016,** *28*, 6804-6834.
13. Fu, Y.;Zhu, H.;Schrader, A. W.;Liang, D.;Jin, S. Nanowire lasers of formamidinium lead halide perovskites and their stabilized alloys with improved stability. *Nano.Lett.* **2016,** *16*, 1000-1008.
14. Zhu, H.;Fu, Y.;Meng, F.;Wu, X.;Gong, Z.;Ding, Q.;Gustafsson, M. V.;Trinh, M. T.;Jin, S.;Zhu, X. Lead halide perovskite nanowire lasers with low lasing thresholds and high quality factors. *Nat. Mater.* **2015,** *14*, 636-642.
15. Xing, G.;Mathews, N.;Lim, S. Low-temperature solution-processed wavelength-tunable perovskites for lasing. *Nat.Mater.* **2014,** *13*, 476-480.
16. Zhong, Q.;Cao, M.;Hu, H.;Di, Y.;Chen, M.;Li, P.;Wu, L.;Qiao, Z. One-pot synthesis of highly stable $CsPbBr_3$@SiO_2 core-shell nanoparticles. *Acs Nano* **2018,** *12*, 8579-8587.
17. Protesescu, L.;Yakunin, S.;Bodnarchuk, M. Nanocrystals of cesium lead halide perovskites ($CsPbX_3$, X = Cl, Br, and I): novel optoelectronic materials showing bright emission with wide color gamut. *Nano.Lett.* **2015,** *15*, 3692-3696.
18. Xu, Y. F.;Yang, M. Z.;Chen, H. Y.;Liao, J. F.;Kuang, D. Enhanced solar-driven gaseous CO_2 conversion by $CsPbBr_3$ nanocrystal/Pd nanosheet Schottky-junction photocatalyst. *ACS Appl. Energy Mater.* **2018,** *1*, 5083-5089.
19. Nedelcu, G.;Protesescu, L.;Yakunin, S.;Bodnarchuk, M. I.;Grotevent, M. J.;Kovalenko, M. Fast anion-exchange in highly luminescent nanocrystals of cesium lead halide perovskites ($CsPbX_3$, X = Cl, Br, I). *Nano Lett.* **2015,** *15*, 5635-5640.
20. Zhang, H.;Wang, X.;Liao, Q., Embedding perovskite nanocrystals into a polymer matrix for tunable luminescence probes in cell imaging *Adv. Funct. Mater.* **2017,** *27*, 1604382.
21. Wei,Y.; Deng, X.;Xie, Z.; Cai, X.; Ma, S. Enhancing the stability of perovskite quantum dots by encapsulation in crosslinked polystyrene beads via a swelling-shrinking strategy toward superior water resistance. *Adv. Funct. Mater.* **2017,** *27*, 1703535.
22. Wang, Y.;Zhu, Y.;Huang, J.;Cai, J.;Zhu, J.;Yang, X.;Shen, J.;Jiang, H.;Li, C. $CsPbBr_3$ perovskite quantum dots-bsed monolithic electrospun fiber membrane as an ultrastable and utrasensitive fluorescent sensor in aqueous medium. *J.Phys. Chem. Lett.* **2016,** *7*, 4253-4258.
23. Raja, S. N.;Bekenstein, Y.;Koc, M. A.;Fischer, S.;Zhang, D.;Lin, L.;Ritchie, R. O.;Yang, P.;Alivisatos, A. Interfaces, Encapsulation of perovskite nanocrystals into macroscale polymer matrices: enhanced stability and polarization. *ACS Appl. Mater. Inter.Inter.* **2016,** *8*, 35523-35533.
24. Hou, S.;Guo, Y.;Tang, Y.;Quan, Q. Interfaces, synthesis and stabilization of colloidal perovskite nanocrystals by multidentate polymer micelles. *ACS Appl. Mater. Inter.* **2017,** *9*, 18417.
25. Liao, H.;Guo, S.;Cao, S.;Wang, L.;Gao, F.;Yang, Z.;Zheng, J.;Yang, W.General strategy for In situ growth of all-Inorganic $CsPbX_3$ (X = Br, I, and Cl) perovskite nanocrystals in polymer fibers toward significantly enhanced water/thermal stabilities. *Adv. Opt. Mater.* **2018,** *6* (15), 1800346.
26. Yang, X.;Xu, T.;Zhu, Y.;Cai, J.;Gu, K; Zhu, J. Devices, E., Preparation of $CsPbBr_3$@PS composite microspheres with high stability by electrospraying. *J. Mater. Chem. C* **2018,** *6*, 7971-7975.
27. Meyns, M.;Perálvarez, M.;Heuer-Jungemann, A.;Hertog, W.;Ibáñez, M.;Nafria, R.;Genç, A.;Arbiol, J.;Kovalenko, M. V.;Carreras, J. Interfaces, polymer-enhanced stability of inorganic perovskite nanocrystals and their application in color conversion LEDs. *ACS Appl. Mat.Inte.* **2016,** *8*, 19579-19586.
28. Li, Z.;Long, K.;Huang, S.;Liang, L. Highly luminescent and ultrastable $CsPbBr_3$ perovskite quantum dots incorporated into a silica/alumina monolith. *Angew. Chem.* **2017,** *129*, 8246-8250.
29. Wang, H. C.;Lin, S. Y.;Tang, A. C.;Singh, B. P.;Tong, H. C.;Chen, C. Y.;Lee, Y. C.;Tsai, T. L.;Liu, S. Mesoporous silica particles integrated with all-Inorganic $CsPbBr_3$ perovskite quantum-dot nanocomposites (MP-PQDs) with high stability and wide color gamut used for backlight display. *Angew. Chem. Int. Ed.* **2016,** *55*, 7924-7929.
30. Dirin, D. N.;Protesescu, L.;Trummer, D.;Kochetygov, I. V.;Yakunin, S.;Krumeich, F.;Stadie, N. P.;Kovalenko, M. V. Harnessing defect-tolerance at the nanoscale: highly luminescent lead halide perovskite nanocrystals in mesoporous silica matrixes. *Nano Lett.* **2016,** *16*, 5866-5874.
31. Chun;Sun;Yu;Zhang;Cheng;Ruan;Chunyang;Yin;Xiaoyong;Materials, W. Efficient and stable white lEDs with silica-coated inorganic perovskite quantum dots. *Adv. Mater.* **2016,** *28*, 10088-10094.
32. Loiudice, A.;Saris, S.;Oveisi, E.;Alexander, D.;Buonsanti, R. $CsPbBr_3$ QD/AlOx inorganic nanocomposites with exceptional stability in water, light, and heat. *Angew. Chem.* **2017,** *129*, 10696-10701.
33. Li, Z.;Hofman, E;Li, J.; Davis A. Photoelectrochemically active and environmentally stable $CsPbBr_3/TiO_2$ core/shell nanocrystals. *Adv. Funct. Mater.* **2017,** *28*, 1704288.

 doi:10.20944/preprints202306.0442.v1

34. Ji, Y.;Wang, M.;Yang, Z.;Qiu, H.;Bhatti, A. Trioctylphosphine-assisted pre-protection low-temperature solvothermal synthesis of highly stable $CsPbBr_3/TiO_2$ Nanocomposites. *J. Phys. Chem. Lett.* **2021,** *12* (15), 3786-3794.
35. Long, R.;Fang, W. H.;Prezhd, O. V. Strong interaction at the perovskite/TiO_2 interface facilitates ultrafast photoinduced charge separation: a nonadiabatic molecular dynamics sudy. *J. Phys. Chem. C* **2017,** *121*.3797-3806.
36. Zhang, Y.;Wang, X.;Chen, Y.;Gao, Y. Improved electroluminescence performance of quantum dot light-emitting diodes: A promising hole injection layer of Fe-doped NiO nanocrystals. *Opt. Mater.* **2020,** *107*, 110158.